Geophysical Research Letters

RESEARCH LETTER
10.1029/2019GL082473

Initial ^{40}Ar-^{39}Ar Ages of the Paleocene-Eocene Boundary Impact Spherules

Morgan F. Schaller[1], Brent D. Turrin[2], Megan K. Fung[1], Miriam E. Katz[1], and Carl C. Swisher[2]

[1]Earth and Environmental Sciences, Rensselaer Polytechnic Institute, Troy, NY, USA, [2]Earth and Planetary Sciences, Rutgers University, Piscataway, NJ, USA

Key Points:
- Radiometric age of P-E boundary impact spherules is 54.2 ± 2.5 Ma, consistent with their depositional age
- Their origin as reworked K-Pg ejecta is not supported by these data

Supporting Information:
- Supporting Information S1
- Figure S1
- Figure S2
- Figure S3
- Data Set S1

Correspondence to:
M. F. Schaller,
schall@rpi.edu

Citation:
Schaller, M. F., Turrin, B. D., Fung, M. K., Katz, M. E., & Swisher, C. C. (2019). Initial ^{40}Ar-^{39}Ar Ages of the Paleocene-Eocene Boundary Impact Spherules. *Geophysical Research Letters*, *46*. https://doi.org/10.1029/2019GL082473

Received 15 FEB 2019
Accepted 8 JUL 2019
Accepted article online 23 JUL 2019

Abstract We report ^{40}Ar-^{39}Ar step-heating ages of Paleocene-Eocene (P-E) boundary impact spherules from Atlantic Margin coastal plain and open ocean sites. We test the hypothesis that the P-E spherules are reworked from an earlier event (e.g., K-Pg impact at ~66 Ma), which predicts a cooling age discordant from their depositional age of 55.93 ± 0.05 Ma at the P-E boundary. Isochrons from the step-heating analysis yield ^{40}Ar-^{36}Ar intercepts in excess of the modern in most cases, indicating that the spherules have excess radiogenic Ar (^{40}Ar*), typical of impact glasses incompletely degassed before solidification. The weighted mean of the isochron-corrected plateau age is 54.2 ± 2.5 Ma (1σ), and their isochron age is 55.4 ± 4.0 Ma, both indistinguishable from their P-E depositional age, not supporting the K-Pg reworking hypothesis. This is consistent with all other stratigraphic and geochemical evidence for an impact at the P-E boundary and ejecta distribution by air fall.

Plain Language Summary We show that the radioisotopic ages of the recently discovered Paleocene-Eocene (P-E) boundary impact melt spherules (54.2 ± 2.5 Ma) are indistinguishable from their depositional age (55.93 ± 0.05 Ma). These initial data indicate that the material is unlikely to have been reworked from some earlier event and hence accompany the climate change at the P-E transition. These air-fall ejecta are the most isochronous P-E horizon available. Inherited radiogenic ^{40}Ar in the spherules is consistent with a P-E impact site at the Marquez Dome crater (eastern Texas); these carbonates overlie petroleum deposits that could have contributed ^{12}C-enriched carbon to the atmosphere upon impact.

1. Introduction

The Paleocene-Eocene (P-E) boundary (56.0 Ma; Gradstein & Ogg, 2012, time scale) is marked by the onset of a carbon isotope excursion (CIE) observed globally (Aubry et al., 2007). This marine CIE, first described by Kennett and Stott (1991) at Site 690 in the Southern Ocean, is associated with a global benthic foraminiferal extinction (see Thomas, 2007, for review). The rapid δ^{13}C excursion is observed globally in both organic and inorganic marine and terrestrial carbon reservoirs (Koch et al., 1992), is accompanied by ~5 °C global warming and widespread ocean acidification (Zachos et al., 2005), and changes in terrestrial mammal and plant assemblages (McInerney & Wing, 2011; Wing et al., 2005). The P-E thermal maximum (PETM) event is often cited as an analog for anthropogenic climate change and has been the focus of decades of research. Among myriad proposed triggers for the rapid event (see McInerney & Wing, 2011, for review), an extraterrestrial impact (Cramer & Kent, 2005; Kent et al., 2003) has more recently garnered renewed interest upon the discovery of extraterrestrial impact ejecta within the CIE onset (Figure 1). Schaller et al. (2016) identified glass spherules within the P-E boundary CIE that meet all the criteria of impact ejecta, including their unique chemical compositions, and inclusions of high-temperature quartz glass (lechatelierite) and shocked quartz grains. In addition, the glass spherules have all the characteristics of air-fall deposition.

The ejecta origin of the material has not been disputed, and it occurs in a restricted stratigraphic interval at Wilson Lake B and Millville (Ocean Drilling Program [ODP] 174AX on the Atlantic Coastal Plain; Miller et al., 2017; Sugarman et al., 2005), a natural P-E boundary exposure near Medford, NJ, and Site 1051B in the open ocean, consistent with air fall (Figure 1). However, because the material is found on the coastal plain at the base of the thick Marlboro Clay unit, which is associated with increased terrigenous sedimentation (Fung et al., 2019; Lanci et al., 2002; Makarova et al., 2017; Schaller & Fung, 2018), there is an underlying concern that the spherules may be reworked ejecta from an earlier impact (e.g., the K-Pg). This "reworking hypothesis" implies that the cooling age of the microtektites is substantially different

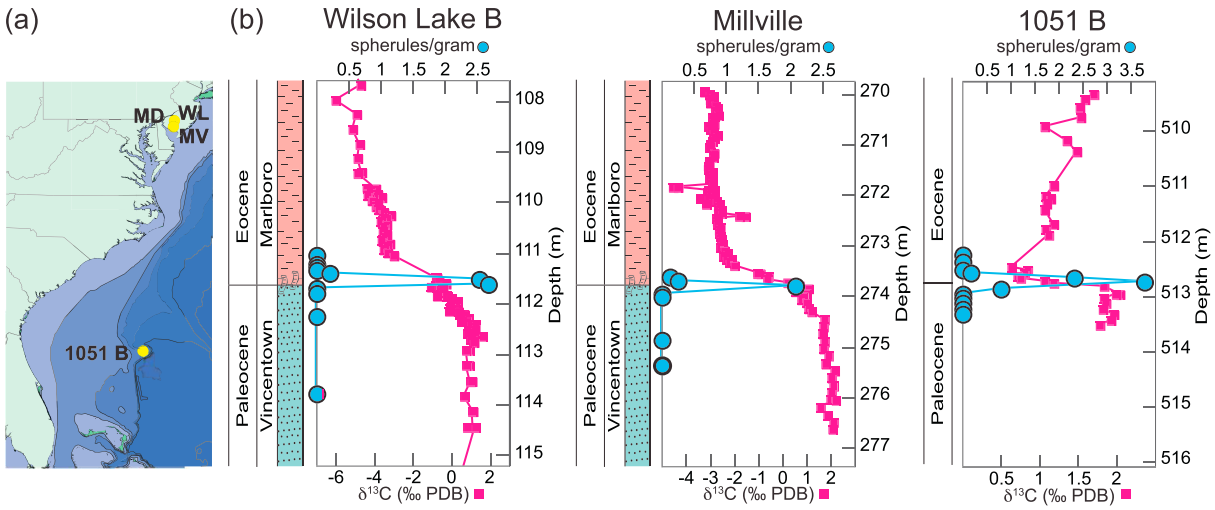

Figure 1. (a) Map showing Atlantic margin locations (Wilson Lake B [WL] and Millville [MV]), as well as an exposure in Medford (MD), NJ, and Site 1051, Blake Nose. (b) Stratigraphic distribution of Paleocene-Eocene (P-E) spherules (blue) from WL, MV, and 1051B (Schaller et al., 2016) compared with the carbon isotope excursion (pink). The bulk carbonate $\delta^{13}C$ from WL and MV is from Wright and Schaller (2013), and Site 1051B is from Katz et al. (1999).

than their apparent depositional age of 55.93 ± 0.05 Ma at the P-E boundary; in this study, we test this hypothesis. Ancillary evidence is inconsistent with the reworking hypothesis: (a) Bulk chemical composition of P-E boundary ejecta is different than the K-Pg ejecta; and (b) P-E boundary spherules were found at Site 1051B, which is in the open ocean (~1,900-m water depth) and unlikely to have had a major coarse-grained terrigenous sediment influx. This ancillary evidence led us to conduct a more conclusive test—radioisotopic dates on the ejecta. Here we present 11 new ^{40}Ar-^{39}Ar radiometric ages (nine step heating, one ^{40}Ar-^{39}Ar total fusion, and one K-Ar) on the P-E spherules that reveal a cooling age that is indistinguishable from the depositional age of the material.

2. P-E Boundary Age

The P-E boundary is marked by the onset of the CIE (Aubry et al., 2007), which is observed globally and can be offset in bulk sediments and foraminifera measured in the same samples (Thomas et al., 2002). The age of the P-E boundary has been estimated by integrating radiometric dates on earliest Eocene ashes with cyclostratigraphy (Charles et al., 2011; Westerhold et al., 2015, 2012, 2009), but the exact age of the CIE onset is not known by absolute dating techniques. The basis for the age of the CIE are ^{40}Ar-^{39}Ar dates from an ash in the Fur Formation that is correlated to the "−17 ash" in ODP Site 550 (Storey et al., 2007), where Westerhold et al. (2015) used cyclostratigraphy to arrive at an age of 55.93 ± 0.05 Ma for the CIE onset at that site. However, both the −17 and +19 ashes fall well above the recovery of the CIE and hence only put an astronomical age on the boundary itself. A bentonite in the "core" of the CIE at Spitsbergen is dated to 55.785 Ma using U-Pb on single-zircon crystals and then used to cyclostratigraphically constrain the CIE onset to 55.866 ± 0.098 Ma (Charles et al., 2011). As far as we are aware, this U-Pb-dated bentonite is stratigraphically the closest published absolute date to the CIE onset and appears to agree with Westerhold et al.'s (2015) age for the boundary. Jaramillo et al. (2010) used U-Pb to date zircon crystals in a pyroclastic tuff at the level of a CIE on the Venezuelan coastal plain to 56.09 ± 0.03 Ma, which is suggested to be the onset of the P-E CIE. However, the CIE does not manifest in its typical form at this site, and the "tuffaceous sandstone" containing the zircons appears to be above the onset of the CIE, within the excursion body. It is possible that this ash layer is reworked, which would explain the discrepancy between the Charles et al. (2011) and Jaramillo et al. (2010) dates.

The glass spherules (microtektites and microkrystites) in the CIE onset (Schaller et al., 2016; Figure 1) provide the means to radiometrically date the P-E boundary directly using ^{40}Ar-^{39}Ar, which is among the most reliable isotope dating methods for impact ejecta (Jourdan et al., 2007). Because the precision on the microtektite ages reported in this paper is well outside the bounds necessary to revisit the age of the CIE onset, we do not address the age of the P-E boundary in this contribution. This is in part because the K content of the P-

Table 1
Summary of Major Element Chemistries (in Stoichiometric Weight Percent) Measured by Wavelength Dispersive X-ray Spectroscopy on Polished Cross Sections of 19 Spherules From Wilson Lake B, Millville, and Site 1051B (Data From Schaller & Fung, 2018)

	SiO_2	Al_2O_3	FeO	MgO	K_2O	CaO	TiO_2	Na_2O
Microkrystite, mean ± 1 *SD* ($n = 5$)	38.06 ± 3.71	18.36 ± 0.90	7.95 ± 1.64	5.67 ± 1.72	0.21 ± 0.08	23.26 ± 2.58	1.5 ± 0.19	0.79 ± 0.38
Microtektite, mean ± 1 *SD* ($n = 14$)	36.87 ± 1.69	18.29 ± 0.33	7.58 ± 0.79	5.34 ± 0.21	0.25 ± 0.16	24.08 ± 2.31	1.62 ± 0.07	1.13 ± 0.44

Note. None of these spherules were measured in this study because of their size and K contents; it was not feasible to cross section the material to be dated.

E spherules is very low (generally <0.5 wt.%; see Table 1; Schaller & Fung, 2018) and their sizes are relatively small (average 302-μm diameter at the Atlantic Coastal Plain sites and 274 μm at Site 1051B; Schaller et al., 2016), making dating individual grains by ^{40}Ar-^{39}Ar an analytical challenge. Rather, the ^{40}Ar-^{39}Ar analyses provide the means to establish whether the cooling age of the spherules is consistent with their depositional age, thereby testing the hypothesis presented above. Work on refining the precision of microtektite ^{40}Ar-^{39}Ar dates using a much larger population of grains is ongoing, but because of the critical nature of the current findings, we report our first round of age determinations here.

3. Argon-Isotope Measurements and ^{40}Ar-^{39}Ar Age Determinations

For the first round of dating P-E ejecta material, 11 spherules were selected from coastal plain sites at Wilson Lake B (ODP 174AX; 39.6598°N, 75.0472W°), Medford, Millville (ODP 174AX; 39.4046°N, 75.0889°W), and open-ocean ODP Site 1051B at Blake Nose (ODP 171B 30.0531°N, 76.3578°W; Figure 1). Though it is difficult to distinguish microtektites (glasses) from microkrystites (containing crystallites) from their exteriors, we included both ejecta forms in our irradiation and analyses. We dated spherules that ranged from ~280 to 100 μm in diameter, with weights between 10 and 50 μg. The total K content measured on a suite of P-E spherules is between 0.21% and 0.25% (Table 1; Schaller & Fung, 2018), which equates to expected ^{39}Ar yields in the attomole to low-femtomole range (10^{-16} to 10^{-15} moles). Such small grains with low K content present a unique analytical challenge.

Argon-isotope measurements were conducted at Rutgers University on an upgraded Mass Analyzer Products 215–50 noble gas mass spectrometer following procedures given in Turrin et al. (2010), Lindsay et al. (2015), and Lindsay et al. (2014). Details are given in electronic supplement.

4. Irradiation and Standards

The P-E glass spherules, along with the reference standards, Fish Canyon sanidine (28.201 Ma; Kuiper et al., 2008), Hb3Gr hornblende (1,080 Ma; Jourdan & Renne, 2007), and the Fire Clay sanidine U-Pb dated at 314.6 ± 0.9 Ma (Lyons et al., 2006) were loaded into pits drilled into a 1-cm-diameter Al disks for neutron irradiation. The pits are arranged in a controlled geometry to facilitate the correction of any measurable gradients in the neutron flux. Neutron irradiation was carried out at the United States Geological Survey TRIGA reactor for 80 hr, without Cd shielding, producing a nominal J values of 1.95×10^{-2}.

For all of the ages reported here, uncertainties are expressed as 1σ unless otherwise specified, and we use the following symbols and constants: Ar* = radiogenic argon; $^{39}Ar = {}^{39}Ar$ produced from ^{39}K; $\lambda = 5.81 \times 10^{-11}$ a^{-1}; $\lambda = K_{\varepsilon\beta}$ 4.962×10^{-10} a^{-1}; $^{40}K/K_{total} = 1.167 \times 10^{-4}$ (Steiger and Jäger, 1977); $^{36}Ar_{Ca}/^{37}Ar_{Ca} = (2.57 \pm 0.03) \times 10^{-4}$; $^{39}Ar_{Ca}/^{37}Ar_{Ca} = (6.62 \pm 0.1) \times 10^{-4}$; $^{40}Ar_K/^{39}Ar_K = (9.8 \pm 0.2) \times 10^{-3}$; $^{38}Ar_K/^{39}Ar_K = (1.319 \pm 0.001) \times 10^{-2}$.

5. Results and Discussion

5.1. Ar-Isotope Systematics

A total of 11 samples were analyzed by the $^{40}Ar/^{39}Ar$ method: nine by step heating and two by total fusion. When plotted on isochrons, the Ar isotopic data indicate that the glass spherules have a trapped component that contains variable amounts of excess ^{40}Ar relative to modern atmospheric Ar (Figures 2 and S1 in the supporting information). The variance weighted average $^{40}Ar/^{36}Ar$ ratio of the trapped component from the individual spherules is 334 ± 13 (Figure S2). When all of the isotopic data are cast on a single-isotope correlation diagram (Figure S3), the distribution produces an age of 49 ± 2 Ma with a trapped $^{40}Ar/^{36}Ar$

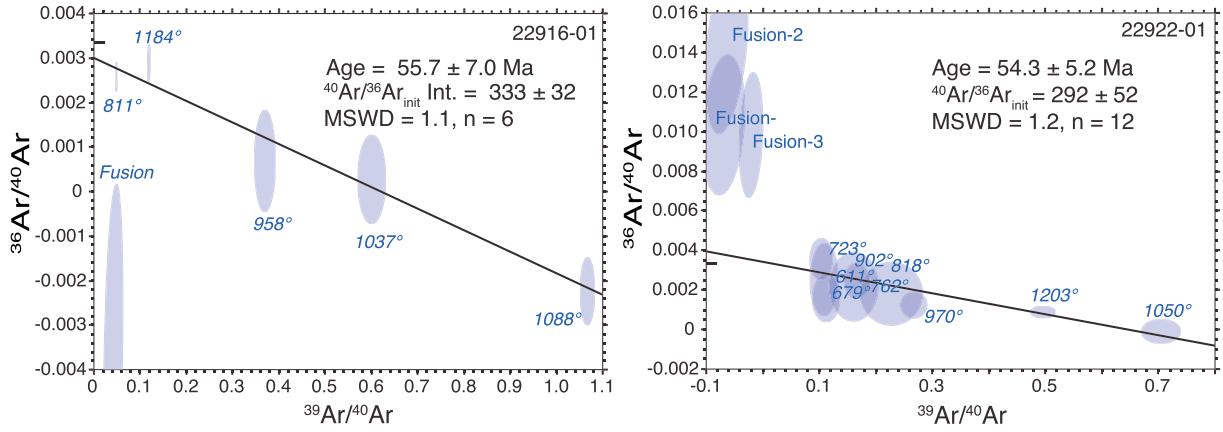

Figure 2. Isochron plots of $^{36}Ar/^{40}Ar$ versus $^{39}Ar/^{40}Ar$ for step-heating samples 22916 and 22922. Temperatures (in °C) are indicated next to each step.

of 321 ± 7 and a mean-square-weighted deviation of 2.8, indicating that there is more dispersion in the 78 data points than can be accounted for by the measurement errors. Applying an outlier elimination algorithm yields a 73-point linear array that corresponds to a $^{40}Ar/^{36}Ar$ value of 313 ± 6 and an age of 50 ± 3 Ma with a mean-square-weighted deviation of 1.1. From these results, we conclude that the trapped Ar in the tektites has a variable $^{40}Ar/^{36}Ar$ ratio.

Despite evidence for the glass spherules having formed above closure temperature (e.g., the presence of lechatelierite with a melting point of ~1,750 °C; see Schaller et al., 2016), postimpact vapor-condensation and/or melt solidification is so rapid that existing radiogenic argon in the melted target rocks is unable to completely degas (Jourdan et al., 2007; Schwarz & Lippolt, 2014). As such, of the nine step-heating results reported here, only two have a trapped component with an $^{40}Ar/^{36}Ar$ ratio close to the presumptive Eocene atmospheric value around 298 (samples 22924 and 22922). The other samples all indicate varying amounts of inherited radiogenic $^{40}Ar^*$, which is typical of ejecta generated from target rocks that are much older than the age of the impact, rather than contemporaneous (Jourdan et al., 2007).

Unlike other impact glasses that show evidence of incomplete degassing (e.g., the Ries impact crater melt glasses; Schwarz & Lippolt, 2014), the $^{36}Ar/^{40}Ar$ versus $^{39}Ar/^{40}Ar$ of each heating step for most of the P-E spherules falls on a simple mixing line (Figures 2 and S1). The isochrons of samples 22879 and 22917 (Figures 2 and S1) show this mixing characteristic. Thus, the low-temperature steps progress along a mixing line from the upper left of the isochron plot to the lower right with increasing temperature and move back along the same mixing line at higher incremental temperature steps. The P-E spherules appear to have only a single component of inherited ^{40}Ar, and the step-heating ages may therefore be corrected using the trapped $^{40}Ar/^{36}Ar$ component (Figure S2).

5.2. Step-Heating Plateau Ages

We determined the plateau steps for the glass spherules (Table 2 and Figure 3). To account for the variable trapped $^{40}Ar/^{36}Ar$ ratio of each spherule, we cast the step-heating data on isochrons where the y-intercept provides the $^{40}Ar/^{36}Ar$ ratio of the trapped component (Table 2 and Figures 2, S1, and S2), which we use to calculate the apparent age for each step. Following Fleck et al. (1977), we calculate the plateau ages using the variance-weighted average of at least three consecutive steps that are analytically indistinguishable at the 95% confidence level and yield $\geq$50% of the total $^{39}Ar_K$ released (Table 2; see discussion of plateau criteria in the Supporting Information). For comparison, we also provide results following the more conventional approach of using the modern atmospheric $^{40}Ar/^{36}Ar$ ratio (298.6) for the trapped component (Table 2).

Nine samples were analyzed by step heating, yielding step-heating cumulative release spectra, K/Ca, and % $^{40}Ar^*$ (Figure 3 and Table 2). In general, the lower temperature steps (~700 to 900 °C) yield smaller Ar signals and comprise the first ~20% or less of the total $^{39}Ar_K$ released. These first steps may represent the differences in degassing of Ar from glassy versus crystalline phases, which are at different relative abundances within each spherule (depending on whether it is a microtektite or a microkrystite; see Schaller et al., 2016).

Geophysical Research Letters

10.1029/2019GL082473

Table 2

Summary Table of $^{40}Ar/^{38}Ar$ Step-Heating and Isochron Ages for the Paleocene-Eocene Boundary Impact Ejecta

Sample	ID	$J \times 10^{-2}$ ($\pm 1\sigma_x$)	Integrated Ca/K ($\pm 1\sigma_x$)	Isochron age ($\pm 1\sigma_x$)	$^{40}Ar/^{36}Ar$ trapped ($\pm 1\sigma_x$)	MSWD	n	Integrated $^{40}Ar^*/^{39}Ar_K$ ($\pm$)	Integrated age $^{40}Ar/^{36}Ar$	% radius	Plateau age ($\pm$1s w/J)	MSWD (plateau)	Steps	n/n_{total}	$\%^{39}Ar$ plateau	Mol $^{39}Ar \times 10^{-15}$	Plateau Ca/K ($\pm$1s)	Comment
WL-365.9	No useful isochron			−16.29 ± 8.1	364 ± 29	0.348	14											Two splits of WL365.9 both small grain-low K microtektites.
	22878-01	1.945 ± 0.001	94.4 ± 6.4		298.60 ± 0.06			1.96 ± 0.57	68 ± 19	15.9	**45 ± 15**	1	B-H	7/8	99.6	0.92	94.9 ± 1.3	No useful isochron for either sample; data too compressed.
	22878-02	1.945 ± 0.001	22.3 ± 1.1		298.60 ± 0.06			1.79 ± 1.49	62 ± 51	15.9	**51 ± 42**	0.1	A-F	6/6	100	0.29	29.0 ± 1.2	Best age estimate assuming modern atmosphere for $^{40}Ar/^{36}Ar_{trap}$.
1051-36-37	22879-01	1.945 ± 0.001	−0.3 ± 0.1	**52.8 ± 12**	551 ± 250	0.624	13	1.88 ± 0.48	65 ± 16	40	**53 ± 9**	0.5	A-L	12/13	99.8	2.25	−9.5 ± 3.5	High-K microtektite. Isochron indicates that $^{40}Ar/^{36}Ar_{trap}$ contains excess ^{40}Ar. Best age estimate, isochron-corrected plat.
	Trapped set to modern atmosphere				298.60 ± 0.06			3.17 ± 0.26	108 ± 8.7	67.4	90.2 ± 4.9	0.9	A-L	12/13	99.8	2.25	−9.5 ± 3.5	
MV-898.8	22916-01	1.945 ± 0.001	88.4 ± 3.4	**55.69 ± 7.3**	333 ± 34	1.103	6	1.70 ± 0.24	58.7 ± 8	80.9	**55.8 ± 7.2**	1	A-F	6/6	100	2.98	67.6 ± 0.9	Isochron indicates that $^{40}Ar/^{36}Ar_{trap}$ is dominantly atmospheric in composition. Best age estimate, isochron-corrected plat.
	Trapped set to modern atmosphere				298.60 ± 0.1			1.74 ± 0.21	60.1 ± 7.2	82.9	55.5 ± 6.5	1.3	A-F	6/6	100	2.98	67.6 ± 0.9	
MV-898.8	22917-01	1.945 ± 0.001	54.2 ± 0.7	35.27 ± 8.7	331 ± 31	0.04	5	1.02 ± 0.30	36 ± 10	40.8	35.5 ± 6.3	0	A-E	5/5	100	1.55	54.8 ± 0.6	Isochron indicates that $^{40}Ar/^{36}Ar_{trap}$ is dominantly atmospheric in composition. Best age estimate, isochron-corrected plat.
	Trapped set to modern atmosphere				298.60 ± 0.1			1.17 ± 0.27	40.6 ± 9.2	46.6	34 ± 5.7	0.4	A-E	5/5	100	1.55	54.8 ± 0.6	
WL-366.2AA	22921-01	1.971 ± 0.001	76.1 ± 1.8	**65.1 ± 27**	494 ± 176	1.475	8	3.71 ± 2.16	127 ± 72	47.3	**54 ± 56**	0.8	D-H	5/8	86.9	0.32	86.9 ± 1.6	Isochron indicates that $^{40}Ar/^{36}Ar_{trap}$ may contain excess ^{40}Ar. Best age estimate, isochron-corrected plat.
	Trapped set to modern atmosphere				298.60 ± 0.1			5.34 ± 1.321	181 ± 43	68.2	47 ± 38	0.1	E-F	2/8	57.2	0.21	88.6 ± 1.9	
MV-898.8AA	22922-01	0.0197136 ± 0.0000729	33.3 ± 0.6	**54.26 ± 5.8**	292 ± 58	1.217	12	2.23 ± 0.26	77.6 ± 8.9	95.8	**53.8 ± 5.4**	0.3	A-I	9/12	98.8	2.81	56.7 ± 0.9	Isochron indicates that $^{40}Ar/^{36}Ar_{trap}$
					298.60 ± 0.1			2.23 ± 0.26	77.5 ± 9	95.8	53.5 ± 5.5	0.3	A-I	9/12	98.8	2.81	56.7 ± 0.9	

Geophysical Research Letters

10.1029/2019GL082473

Table 2 *(continued)*

Sample	ID	$J \times 10^{-2}$ ($\pm 1\sigma_x$)	Integrated Ca/K ($\pm 1\sigma_x$)	Isochron age ($\pm 1\sigma_x$)	$^{40}Ar/^{36}Ar$ trapped ($\pm 1\sigma_x$)	MSWD	n	Integrated $^{40}Ar^*/^{39}Ar_K$ ($\pm$)	Integrated age $^{40}Ar/^{36}Ar$	% radius	Plateau age ($\pm 1s$ w/J)	MSWD (plateau)	Steps	n/ n_{total}	% ^{39}Ar plateau	Mol $^{39}Ar \times 10^{-15}$	Plateau Ca/K ($\pm 1s$)	Comment
																		is dominantly atmospheric in composition. Best age estimate, isochron-corrected plat.
	Trapped set to modern atmosphere																	
MD-0-1.5	22923-01	1.971 ± 0.001	92.0 ± 5.4	**63.6 ± 14**	436 ± 65	0.927	8	1.68 ± 0.57	59 ± 19	53.6	**64 ± 15**	0.9	A-H	8/8	100	1.58	79.9 ± 3.1	Isochron indicates that $^{40}Ar/^{36}Ar_{trap}$ contains excess ^{40}Ar. Best age estimate, isochron-corrected plat.
	Trapped set to modern atmosphere				298.60 ± 0.1			2.14 ± 0.39	75 ± 13	68.2	55 ± 10	0.4	B-H	7/8	99.3	1.58	79.9 ± 3.1	
WL-365.9	22924-01	1.971 ± 0.001	37.4 ± 0.5	**49.4 ± 24**	300 ± 25	0.365	7	1.59 ± 0.40	56 ± 14	10.6	49.5 ± 9.6	0.3	A-G	7/7	100	1.43	39.7 ± 0.5	Isochron indicates that $^{40}Ar/^{36}Ar_{trap}$ is dominantly atmospheric in composition.
	Trapped set to modern atmosphere				298.60 ± 0.1			1.64 ± 0.40	57 ± 14	10.9	**50.8 ± 9.6**	0.3	A-G	7/7	100	1.43	39.7 ± 0.5	
1051-36-37	22926-01	1.971 ± 0.001	99.8 ± 3.1	12.48 ± 9.7	334 ± 52	0.39	6	1.27 ± 2.06	45 ± 71	7.1	15 ± 45	0.3	A-F	6/6	100	0.24	129 ± 3	Isochron indicates that $^{40}Ar/^{36}Ar_{trap}$ is dominantly atmospheric in composition. Best age estimate, isochron-corrected plat.
	Trapped set to modern atmosphere				298.60 ± 0.1			3.02 ± 0.35	104 ± 62	16.9	**54 ± 39**	0.5	A-F	6/6	100	0.24	129 ± 3	
WL-365.9	22925-01	1.971 ± 0.001	80.9 ± 1.8		298.60 ± 0.1			1.52 ± 0.35	**53 ± 9**	33.4	Total fusion. No isochron or plateau age available.							
	Trapped set to modern atmosphere																	
															Mass (μg)	Moles $^{40}Ar^*$	% K^+	See Schaller and Fung (2018)
1051-36-37	**RPI-1601**[a]	Total fusion (unirradiated)			298.60 ± 0.1				**54.9 ± 4**						118	2.25	0.197	
	Trapped set to modern atmosphere																	
Variance weighted mean isochron				55.4 ± 4.0														
Variance weighted mean using $^{40}Ar/^{36}Ar$ trapped from isochrons									59.4 ± 4.5		49.6 ± 3.1							
Variance weighted mean trapped set to atmosphere									62.7 ± 2.6		59.4 ± 2.5							
Variance weighted mean preferred age											**54.2 ± 2.5**[b]							

Note. We compare step-heating results (a) assuming modern atmospheric $^{40}Ar/^{39}Ar$ for trapped component and (b) using $^{40}Ar/^{39}Ar$ trapped determined from isochrons. Ages used for averaging are indicated in bold. All ages are expressed in Ma.

Abbreviations: σ, standard deviation; σ_x, standard error or standard error on the mean; MSWD, mean-square-weighted deviation; RPI, Rensselaer Polytechnic Institute.

[a]Measured on calibrated quadrupole at RPI (see Schaller & Fung, 2018). [b]Preferred age includes both total fusion ages and all plateau ages in bold.

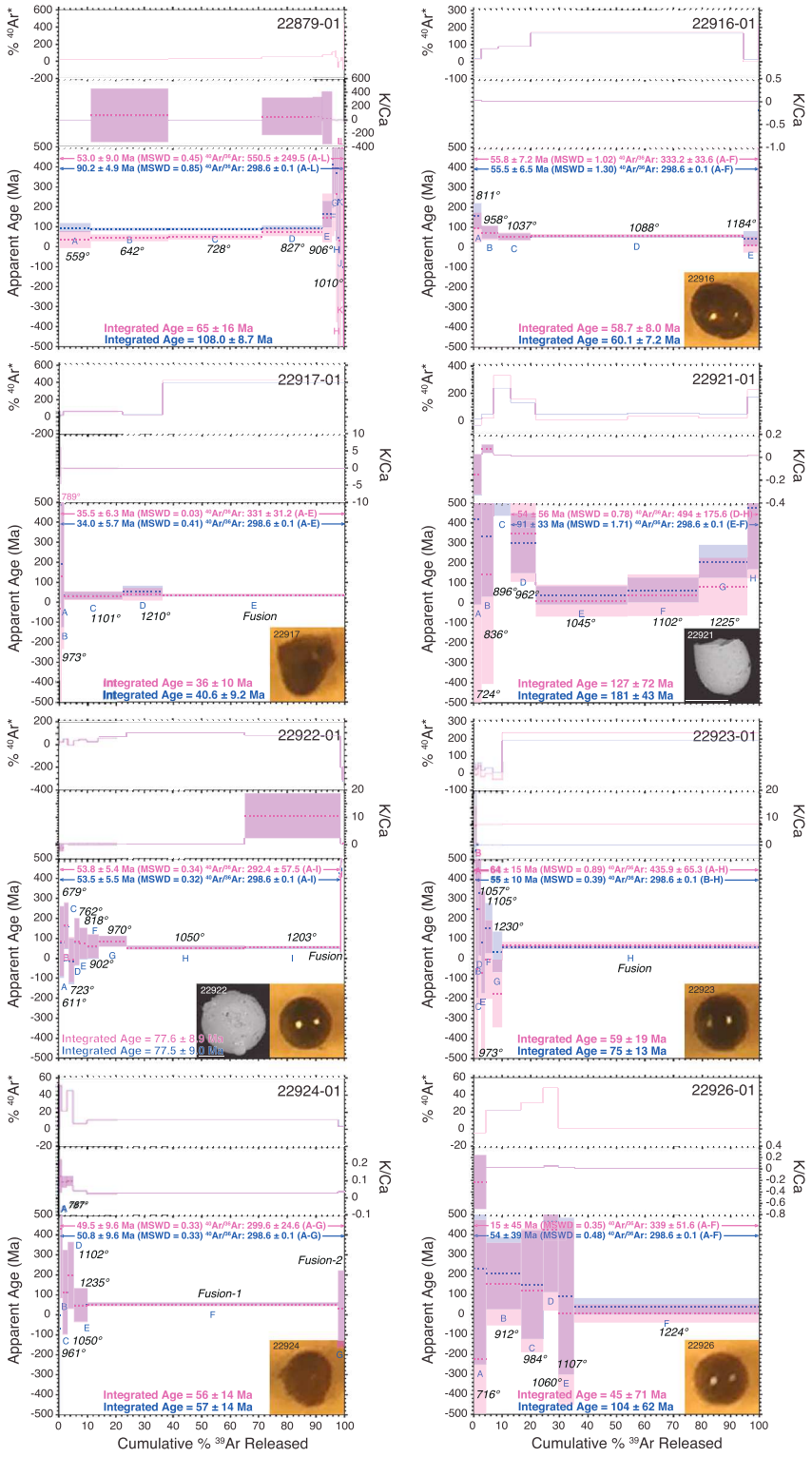

Figure 3. ^{40}Ar-^{39}Ar step-heating diagrams for samples in Table 2. Blue color/dashed lines show the plateau age calculated using the assumed atmospheric initial ratio $^{40}Ar/^{36}Ar = 298.6 \pm 0.2$. Pink color/dashed lines show the plateau age using the trapped $^{40}Ar/^{36}Ar$ determined from corresponding isochrons in Figures 2 and S1 in the supporting information. The plateau ages are calculated using the steps indicated, and the temperatures are indicated in Celsius for each step. Insets are light micrographs or electron backscatter images showing the spherule corresponding to the analysis; scale bar (22921 and 22922) is 200 microns.

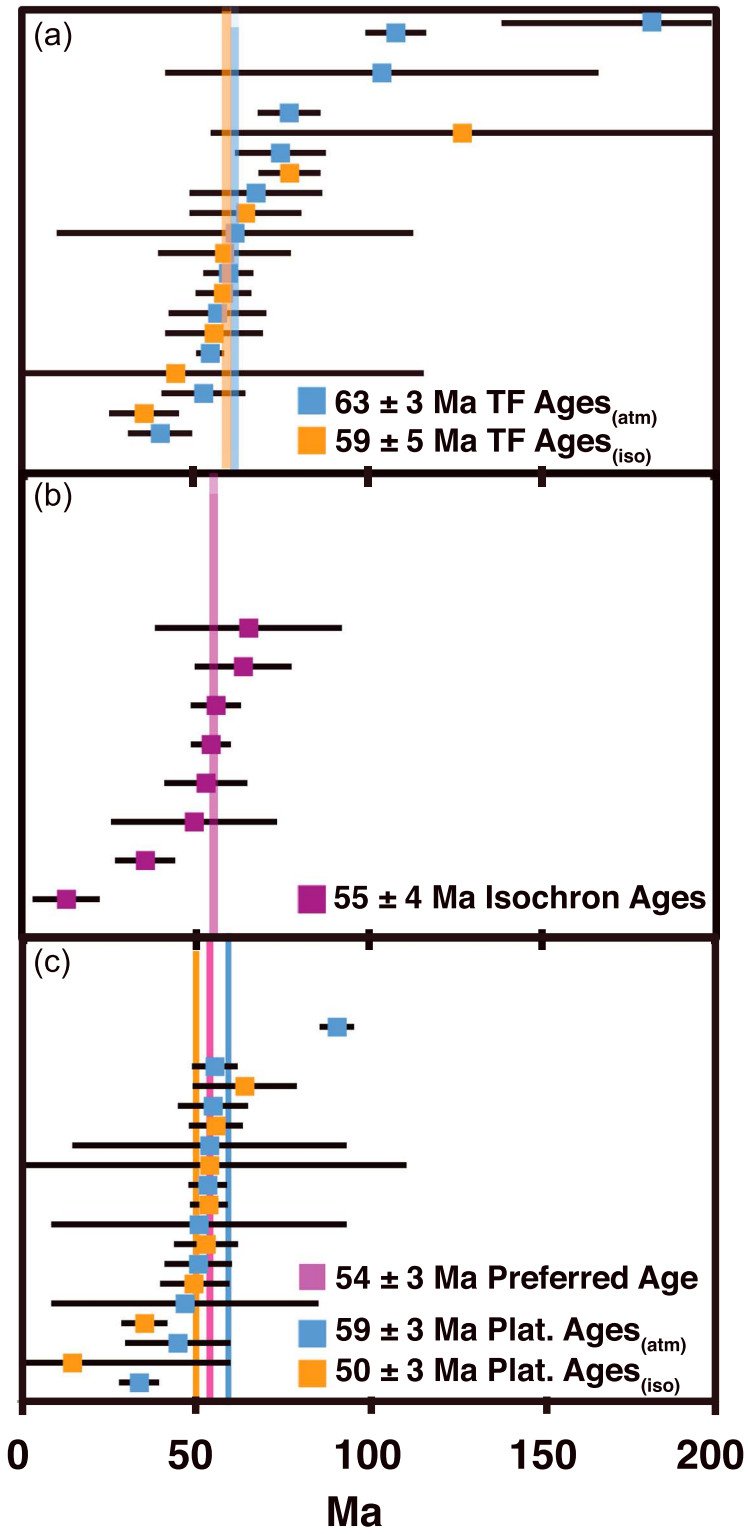

Figure 4. Age distribution summary diagram showing the difference when ages are calculated using an atmospheric $^{40}Ar/^{36}Ar$ of 298.6 (blue) versus the $^{40}Ar/^{36}Ar$ of the trapped component from isochrons (orange) for (a) total fusion and (c) plateaus from step heating. Ages in (b) are from the slope of the iscohrons shown in supporting information Figure S1. Horizontal axis scale is necessarily large to encompass the anomalously old integrated ages in (a). All data are found in Table 2 and S1.

These first steps, representing ~20% of the total gas, have significantly older and more scattered ^{40}Ar-^{39}Ar apparent ages, except in the case of sample 22879, in which the last ~4% of the gas had significantly older apparent ages than the preceding 96%. In contrast, the last ~50% of the $^{39}Ar_K$ is released from the majority of the samples in one or two steps at temperatures of >1,000 °C. This component is most likely from the refractory glass phases of the microtektites (Figure 3).

In addition, samples displaying low-temperature variability in $^{40}Ar/^{39}Ar$ release spectra (22916, 22917, 22922, 22923, 22924, 22926, and 22878) also show more variability in Ca/K, indicating that Ca and K may be heterogeneously distributed and/or partitioned between the glass and crystalline phases within the spherules. The Ar system in the glassy microtektites may be incompletely reset by diffusion before spherule solidification, whereas the microkrystites might be expected to be more fully equilibrated. The disturbed humped and/or saddle-shaped Ar release spectra are fairly typical of incompletely degassed impact glasses (Jourdan et al., 2007; Schwarz & Lippolt, 2014) that carry an inherited ^{40}Ar signal from the target rocks. In general, however, the samples with the highest K/Ca ratios yield the most precise ages (e.g., sample 22922), and almost all the integrated ages are older than the plateau and isochron ages (Figure 4). The weighted average of the integrated ages of this population is 59.4 ± 4.5 Ma when corrected using the $^{40}Ar/^{36}Ar$ ratio determined from the isochrons (Table 2), versus 62.7 ± 2.6 Ma assuming a $^{40}Ar/^{36}Ar$ ratio of 298.6. Notably, the integrated age of glassy sample 22924 (56 ± 14 Ma) is indistinguishable from the total fusion ages of samples 22925 and RPI-1601 (53 ± 12 and 54.9 ± 4 Ma, respectively). Two samples (22917 and 22926) yielded very little total gas, at far less than 1×10^{-16} moles, and were excluded from the average (see Supporting Information).

Because the spherules meet all the criteria of impact ejecta that were generated in the same event (Schaller et al., 2016), we use the weighted average of the ages from the analyzed population of grains. The variance-weighted average of the plateau ages is 59.4 ± 2.5 Ma (1σ) using a uniformly applied modern $^{40}Ar/^{36}Ar$ ratio of 298.6, and 54.2 ± 2.5 Ma (1σ) using the $^{40}Ar/^{36}Ar$ ratios determined from the isochrons as indicated in Table 2 (Figure 4). The cooling age of 54.2 ± 2.5 Ma is indistinguishable from the depositional age of the spherules at the P-E boundary of 55.93 ± 0.05 Ma (Westerhold et al., 2015). These isochron-corrected plateau ages are almost always younger than the integrated ages, again pointing to an incomplete resetting of the Ar-isotope system of the melted target material before solidification in the ejecta, which is typical of impact events.

The $^{40}Ar^*$ excess provides ancillary evidence of the mode of spherule formation in an impact event and gives a clue about the age difference between the target rocks and the impact event. Determining the exact age difference is not feasible given the limited size of the current data set, yet we can surmise that the target rocks were not contemporaneous marine rocks or sediments, because these materials probably would not provide excess radiogenic ^{40}Ar. Early Cretaceous shallow marine carbonate/siliciclastic sedimentary rocks of cratonic origin at the impact site could account for the high Ca content and marine Sr/Ca ratio (Schaller & Fung, 2018) of the spherules, as well as the inherited radiogenic component. Such a lithology would be consistent with the target rocks of the Marquez Dome crater in eastern Texas, which is the remnant of a 12.7-km-diameter impact of P-E age (Buchanan et al., 1998), and has a fission track age of 58 ± 3.1 Ma (McHone & Sorkhabi, 1994). The age of the Marquez crater is currently indistinguishable from the age of the spherules, and hence, any datable impact material proximal to the crater should be revisited with more precise methodology in a future study. It is notable that the Marquez impact crater is within carbonate rocks that overlie petroleum deposits, a potential source for ^{12}C-enriched carbon to be liberated upon impact, which could have contributed to the PETM CIE. This tentative correspondence deserves more thorough investigation in future work.

6. Preliminary Implications for the P-E Boundary

The ^{40}Ar-^{39}Ar age of 54.2 ± 2.5 Ma is crucial for two important reasons: (a) It demonstrates that the depositional age of the P-E ejecta material is indistinguishable from the cooling age of the spherules; and (b) it does not support the hypothesis that the spherules are reworked ejecta material from the K-Pg impact, establishing a record of extraterrestrial impact at the P-E boundary. Although the error envelope on the ^{40}Ar-^{39}Ar age does not completely exclude the possibility that the ejecta are reworked from an impact somewhere in that time window, such a reworking scenario does not explain presence of the spherules at open-ocean Site 1051B

within the onset of the CIE. Lateral transport and redeposition are unlikely to have been significant at an open-ocean site on the Blake Nose. Multiple lines of evidence (benthic foraminiferal assemblages, stable isotopes, trace elements, sedimentology, and *X-ray fluorescence*) indicate that any sediment transported downslope in the PETM section at Site 1051 originated from a penecontemporaneous horizon just upslope immediately below the onset of the CIE (Katz et al., 1999). The radioisotopic age of a spherule from Site 1051 (22879) supports that it is not a reworked K-Pg spherule. Furthermore, the chemistry of the P-E spherules differs significantly from those found at K-Pg boundary sections (Schaller et al., 2016), with the latter having much higher in silica content (45% to 68%; Alvarez et al., 1992) and substantially lower Ca/K ratios (Dalrymple et al., 1993; Swisher et al., 1992). Moreover, there are no anomalous Paleocene microfossils (e.g., foraminifera) deposited along with the spherules that would indicate delivery by lateral transport or reworking. Without any a priori reason to suspect that the depositional age of the spherules is discordant from their cooling age, we conclude that the microtektites were most likely deposited by air fall from an impact at the onset of the CIE.

Because the depositional and cooling ages of the spherules are indistinguishable, the P-E impact ejecta may represent an isochronous marker to which other observations at the P-E boundary may be referenced. If we accept the air-fall ejecta deposit as the most isochronous horizon available, we are freed from the constraint of referencing all other observations at the P-E boundary to the onset of the CIE, which is diachronous depending on the response time of the reservoir in question (e.g., Kirtland Turner & Ridgwell, 2016). This opens up the new possibility of assessing the true leads-lags in C-system response between different surficial carbon reservoirs that react and equilibrate on different time scales. For example, one may reasonably expect that the continental shelves would respond much more rapidly to an atmospheric perturbation than the deep ocean (Chen et al., 2013; Thomas et al., 2004, 2005) but the level of resolution in open-ocean sections is insufficient to address this directly using the CIE recorded at each site. Referencing the CIE to the ejecta layer will make these effects apparent particularly at high sedimentation rate sites and will be the subject for significant further work. In addition, refinement of the age of the ejecta can be accomplished by analyzing five- to ten-fold more spherules with a preference for those with higher K content.

Our results indicate that the P-E spherule horizon is (a) air-fall impact ejecta, (b) primary (not reworked), and (c) likely an isochronous horizon at the P-E boundary. The distribution of the spherules at multiple sites located >1,000 km apart on the Atlantic Coastal Plain in P-E boundary sediments, their related major element chemistries, low volatile contents, and mineralogy, along with the inclusion of shocked quartz grains and high-temperature glasses, establishes that the material is impact ejecta. Their sedimentary distribution and radiometric age indicate that they are not reworked from another impact, that they are air fall, and that their cooling age is indistinguishable from their depositional age. As such, the virtually instantaneous time line created by the spherule horizon provides the most isochronous layer within the P-E boundary CIE that has yet been identified. An important implication of our results is that the stratigraphic superposition of the P-E ejecta within the onset of the carbon-cycle perturbation provides the only physical evidence of a potential forcing mechanism at a critical juncture in Earth's climate history. An important implication of our results is that the stratigraphic superposition of the P-E ejecta within the onset of the carbon-cycle perturbation provides the only physical evidence of a potential forcing mechanism at a critical a juncture in Earth's climate history.

Acknowledgments
We thank Wally Broecker, Richard Alley, Jeff Severinghaus, Dennis Kent, and the Comer Changelings for engaging discussions. We thank IODP for supplying samples. This work was funded by NSF Award 1737100 (M. F. S. and M. E. K). All data accompanying this work are available in the electronic supplement.

References

Alvarez, W., Smit, J., Lowrie, W., Asaro, F., Margolis, S. V., Claeys, P., et al. (1992). Proximal impact deposits at the Cretaceous-Tertiary boundary in the Gulf of Mexico: A restudy of DSDP Leg 77 Sites 536 and 540. *Geology*, *20*, no(8), 697–700.

Aubry, M.-P., Ouda, K., Dupuis, C., Berggren, W. A., Van Couvering, J. A., Ali, J., et al. (2007). The Global Standard Stratotype-section and Point (GSSP) for the base of the Eocene series in the Dababiya section (Egypt). *Episodes*, *30*, no(4), 271–286.

Buchanan, P. C., Koeberl, C., & Reid, A. M. (1998). Impact into unconsolidated, water-rich sediments at the Marquez Dome, Texas. *Meteoritics & Planetary Science*, *33*, no(5), 1053–1064.

Charles, A. J., Condon, D. J., Harding, I. C., Pälike, H., Marshall, J. E. A., Cui, Y., et al. (2011). Constraints on the numerical age of the Paleocene-Eocene boundary. *Geochemistry, Geophysics, Geosystems*, *12*, Q0AA17. https://doi.org/10.1029/2010gc003426

Chen, C.-T., Huang, T.-H., Chen, Y.-C., Bai, Y., He, X., & Kang, Y. (2013). Air-sea exchanges of CO_2 in the world's coastal seas. *Biogeosciences*, *10*, no(10), 6509.

Cramer, B. S., & Kent, D. V. (2005). Bolide summer: The Paleocene/Eocene thermal maximum as a response to an extraterrestrial trigger: Palaeogeography, Palaeoclimatology. *Palaeoecology*, *224*, no(1-3), 144–166. https://doi.org/10.1016/j.palaeo.2005.03.040

Dalrymple, G. B., Izett, G. A., Snee, L. W., & Obradovich, J. D. (1993). *$^{40}Ar/^{39}Ar$ age spectra and total-fusion ages of tektites from Cretaceous-Tertiary boundary sedimentary rocks in the Beloc Formation*. Haiti: US Government Printing Office.

Fleck, R. J., Sutter, J. F., & Elliot, D. H. (1977). Interpretation of discordant $^{40}Ar/^{39}Ar$ age-spectra of Mesozoic tholeiites from Antarctica. *Geochimica et Cosmochimica Acta*, *41*, no(1), 15–32.

Fung, M., Schaller, M., Hoff, C., Katz, M., & Wright, J. (2019). Widespread and intense wildfires at the Paleocene-Eocene boundary. *Geochemical Perspective Letters*, *10*.

Gradstein, F. M., & Ogg, J. G. (2012). Chapter 2—The chronostratigraphic scale. In *the geologic time scale*, (pp. 31–42). Boston: Elsevier.

Jaramillo, C., Ochoa, D., Contreras, L., Pagani, M., Carvajal-Ortiz, H., Pratt, L. M., et al. (2010). Effects of rapid global warming at the Paleocene-Eocene boundary on neotropical vegetation. *Science*, *330*, no(6006), 957–961. https://doi.org/10.1126/science.1193833

Jourdan, F., Renne, P., & Reimold, W. (2007). The problem of inherited $^{40}Ar^*$ in dating impact glass by the $^{40}Ar/^{39}Ar$ method: Evidence from the Tswaing impact crater (South Africa). *Geochimica et Cosmochimica Acta*, *71*, no(5), 1214–1231.

Jourdan, F., & Renne, P. R. (2007). Age calibration of the Fish Canyon sanidine $^{40}Ar/^{39}Ar$ dating standard using primary K-Ar standards. *Geochimica et Cosmochimica Acta*, *71*, no(2), 387–402.

Katz, M. E., Pak, D. K., Dickens, G. R., & Miller, K. G. (1999). The source and fate of massive carbon input during the latest Paleocene thermal maximum. *Science*, *286*, no(5444), 1531–1533. https://doi.org/10.1126/science.286.5444.1531

Kennett, J. P., & Stott, L. D. (1991). Abrupt deep-sea warming, palaeoceanographic changes and benthic extinctions at the end of the Palaeocene. *Nature*, *353*, no(6341), 225–229.

Kent, D. V., Cramer, B. S., Lanci, L., Wang, D., Wright, J. D., & Van der Voo, R. (2003). A case for a comet impact trigger for the Paleocene/Eocene thermal maximum and carbon isotope excursion. *Earth and Planetary Science Letters*, *211*, no(1-2), 13–26.

Kirtland Turner, S., & Ridgwell, A. (2016). Development of a novel empirical framework for interpreting geological carbon isotope excursions, with implications for the rate of carbon injection across the PETM. *Earth and Planetary Science Letters*, *435*, 1–13. https://doi.org/10.1016/j.epsl.2015.11.027

Koch, P. L., Zachos, J. C., & Gingerich, P. D. (1992). Correlation between isotope records in marine and continental carbon reservoirs near the Palaeocene/Eocene boundary. *Nature*, *358*, no(6384), 319–322.

Kuiper, K., Deino, A., Hilgen, F., Krijgsman, W., Renne, P., & Wijbrans, J. (2008). Synchronizing rock clocks of Earth history. *Science*, *320*, no(5875), 500–504. https://doi.org/10.1126/science.1154339

Lanci, L., Kent, D. V., & Miller, K. G. (2002). Detection of Late Cretaceous and Cenozoic sequence boundaries on the Atlantic coastal plain using core log integration of magnetic susceptibility and natural gamma ray measurements at Ancora, New Jersey. *Journal of Geophysical Research*, *107*, no(B10), 2216.

Lindsay, F. N., Delaney, J. S., Herzog, G. F., Turrin, B. D., Park, J., & Swisher, C. C. III (2015). Rheasilvia provenance of the Kapoeta howardite inferred from ~1 Ga $^{40}Ar/^{39}Ar$ feldspar ages. *Earth and Planetary Science Letters*, *413*, 208–213. https://doi.org/10.1016/j.epsl.2014.12.049

Lindsay, F. N., Herzog, G. F., Park, J., Delaney, J. S., Turrin, B. D., & Swisher, C. C. III (2014). $^{40}Ar/^{39}Ar$ dating of microgram feldspar grains from the paired feldspathic achondrites GRA 06128 and 06129. *Geochimica et Cosmochimica Acta*, *129*, 96–110.

Lyons, P. C., Krogh, T., Kwok, Y., Davis, D. W., Outerbridge, W. F., & Evans, H. T. Jr. (2006). Radiometric ages of the Fire Clay tonstein [Pennsylvanian (Upper Carboniferous), Westphalian, Duckmantian]: A comparison of U-Pb zircon single-crystal ages and $^{40}Ar/^{39}Ar$ sanidine single-crystal plateau ages. *International Journal of Coal Geology*, *67*, no(4), 259–266.

Makarova, M., Wright, J. D., Miller, K. G., Babila, T. L., Rosenthal, Y., & Park, J. I. (2017). Hydrographic and ecologic implications of foraminiferal stable isotopic response across the US mid-Atlantic continental shelf during the Paleocene-Eocene thermal maximum. *Paleoceanography*, *32*, 56–73. https://doi.org/10.1002/2016PA002985

McHone, J., & Sorkhabi, R. (1994, Volume). Apatite fission-track age of Marquez Dome impact structure, Texas. *in Proceedings Lunar and Planetary Science Conference*, *25*, 881.

McInerney, F. A., & Wing, S. L. (2011). The Paleocene-Eocene thermal maximum: A perturbation of carbon cycle, climate, and biosphere with implications for the future. *Annual Review of Earth and Planetary Sciences, 39*, pp. 489–516.

Miller, K. G., Browning, J. V., Aubry, M.-P., Babila, T., Baluyot, R. D., Esmeray-Senlet, S., et al. (2017). Wilson Lake site, Proceedings of the Ocean Drilling Program, Initial Reports 174AX.

Schaller, M. F., & Fung, M. K. (2018). The extraterrestrial impact evidence at the Palaeocene-Eocene boundary and sequence of environmental change on the continental shelf. *Philosophical Transactions of the Royal Society A: Mathematical, Physical and Engineering Sciences*, *376*, no(2130), 20170081. https://doi.org/10.1098/rsta.2017.0081

Schaller, M. F., Fung, M. K., Wright, J. D., Katz, M. E., & Kent, D. V. (2016). Impact ejecta at the Paleocene-Eocene boundary. *Science*, *354*, no(6309), 225–229. https://doi.org/10.1126/science.aaf5466

Schwarz, W. H., & Lippolt, H. J. (2014). ^{40}Ar-^{39}Ar step-heating of impact glasses from the Nördlinger Ries impact crater—Implications on excess argon in impact melts and tektites. *Meteoritics & Planetary Science*, *49*(6), 1023–1036.

Steiger, R. H., & Jäger, E. (1977). Subcommission on geochronology: convention on the use of decay constants in geo-and cosmochronology. *Earth and Planetary Science Letters*, *36*(3), 359–362.

Storey, M., Duncan, R. A., & Swisher, C. C. (2007). Paleocene-Eocene thermal maximum and the opening of the northeast Atlantic. *Science*, *316*, no(5824), 587–589. https://doi.org/10.1126/science.1135274

Sugarman, P. J., Miller, K. G., Browning, J. V., McLaughlin, P. P. Jr., Brenner, G. J., Buttari, B., et al. (2005). 5. Millville Site. In K. G. Miller, P. J. Sugarman, J. V. Browning, et al. (Eds.), *Proceedings of the Ocean Drilling Program, Initial Reports*, 174AX, (pp. 1–94). College Station, TX: Ocean Drilling Program. https://doi.org/10.2973/odp.proc.ir.174axs.106.2005

Swisher, C. C., Grajales-Nishimura, J. M., Montanari, A., Margolis, S. V., Claeys, P., Alvarez, W., et al. (1992). Coeval $^{40}Ar/^{39}Ar$ ages of 65.0 million years ago from Chicxulub crater melt rock and Cretaceous-Tertiary boundary tektites. *Science*, *257*, no(5072), 954–958.

Thomas, D. J., Zachos, J. C., Bralower, T. J., Thomas, E., & Bohaty, S. (2002). Warming the fuel for the fire: Evidence for the thermal dissociation of methane hydrate during the Paleocene-Eocene thermal maximum. *Geology*, *30*, no(12), 1067–1070.

Thomas, E. (2007). Cenozoic mass extinctions in the deep sea: What perturbs the largest habitat on Earth? *Geological Society of America Special Papers*, *424*, 1–23.

Thomas, H., Bozec, Y., Elkalay, K., De Baar, H., Borges, A., & Schiettecatte, L.-S. (2005). Controls of the surface water partial pressure of CO_2 in the North Sea. *Biogeosciences*, *2*, no(4).

Thomas, H., Bozec, Y., Elkalay, K., & de Baar, H. J. W. (2004). Enhanced open ocean storage of CO_2 from shelf sea pumping. *Science*, *304*, no(5673), 1005–1008.

Turrin, B. D., Swisher, C. C., & Deino, A. L. (2010). Mass discrimination monitoring and intercalibration of dual collectors in noble gas mass spectrometer systems. *Geochemistry, Geophysics, Geosystems*, *11*, Q0AA09. https://doi.org/10.1029/2009GC003013

Westerhold, T., Röhl, U., Frederichs, T., Bohaty, S., & Zachos, J. (2015). Astronomical calibration of the geological timescale: Closing the middle Eocene gap. *Climate of the Past*, *11*, no(9), 1181–1195.

Westerhold, T., Röhl, U., & Laskar, J. (2012). Time scale controversy: Accurate orbital calibration of the early Paleogene. *Geochemistry, Geophysics, Geosystems*, *13*, Q06015. https://doi.org/10.1029/2012GC004096

Westerhold, T., Röhl, U., McCarren, H. K., & Zachos, J. C. (2009). Latest on the absolute age of the Paleocene-Eocene thermal maximum (PETM): New insights from exact stratigraphic position of key ash layers +19 and −17. *Earth and Planetary Science Letters*, *287*, no(3-4), 412–419. https://doi.org/10.1016/j.epsl.2009.08.027

Wing, S. L., Harrington, G. J., Smith, F. A., Bloch, J. I., Boyer, D. M., & Freeman, K. H. (2005). Transient floral change and rapid global warming at the Paleocene-Eocene boundary. *Science*, *310*, no(5750), 993–996. https://doi.org/10.1126/science.1116913

Wright, J. D., & Schaller, M. F. (2013). Evidence for a rapid release of carbon at the Paleocene-Eocene thermal maximum: Proceedings of the National Academy of Sciences, *110*(40), 15,908–15,913.

Zachos, J. C., Rohl, U., Schellenberg, S. A., Sluijs, A., Hodell, D. A., Kelly, D. C., et al. (2005). Rapid acidification of the ocean during the Paleocene-Eocene thermal maximum. *Science*, *308*, no(5728), 1611–1615.